Ultraviolet photodetectors based on selectively grown ZnO nanorod arrays

L. W. Ji,[1,a] S. M. Peng,[2] Y. K. Su,[2] S. J. Young,[2] C. Z. Wu,[1] and W. B. Cheng[1]
[1]*Institute of Electro-Optical and Materials Science, National Formosa University, Yunlin 632, Taiwan*
[2]*Institute of Microelectronics and Department of Electrical Engineering, National Cheng Kung University, Tainan 701, Taiwan*

(Received 20 January 2009; accepted 30 April 2009; published online 20 May 2009)

Metal-semiconductor-metal (MSM) ultraviolet (UV) photodetectors with ZnO nanorods (NRs) have been fabricated and characterized in this investigation. The NR arrays were selectively grown on the gap of interdigitated electrodes by chemical solution method through a photolithography process. Compared to a traditional ZnO MSM photodetector with no NRs, the fabricated NR UV photodetector showed much higher photoresponsity. As a result, it can be attributed to high surface-to-volume ratio of ZnO NRs and such a high photoresponse could strongly depend on oxygen adsorption/desorption process in the presence of trap states at the NR surface. © *2009 American Institute of Physics*. [DOI: 10.1063/1.3141447]

ZnO-based semiconductors have been recognized as a very promising material for optoelectronic applications in the ultraviolet (UV) region due to its large exciton binding energy of 60 meV and wide bandgap energy of 3.37 eV at room temperature.[1–4] In the past decade, one-dimensional ZnO nanostructures[5,6] have been demonstrated a variety of functional device applications, such as light-emitting diodes,[7] nanolasers,[8] photodetectors (PDs),[9–11] field-effect transistors (FET),[12,13] photovoltaic devices,[14] nanogenerators,[15] chemical sensors,[16] etc.

In this work, we report the fabrication and characterization of a metal-semiconductor-metal (MSM) UV PDs with ZnO nanorods (NRs). The NR arrays were selectively grown on the gap of interdigitated electrodes by chemical solution method through a photolithography process. We found the fabricated NR UV PDs demonstrated a higher photoresponse and UV-to-visible rejection ratio than the traditional ZnO MSM PDs.

Before the device fabrication, 40-nm-thick ZnO seed layers were deposited onto glass substrates using radio frequency magnetron sputter deposition technique. Sequentially the as-grown ZnO films were annealed at 450 °C for 30 min under oxygen ambience. 120-nm-thick Ag electrodes were subsequently deposited onto the ZnO film by electron beam evaporation to serve as Schottky contacts. The fingers of the Ag contact electrodes were 150 μm long and 10 μm wide with 10 μm spacing. The active area of the whole device was 150×160 μm^2. Then we employed the photoresists in protecting the electrode patterns by lithography technique. The sample with photoresist-protected interdigitated electrodes was subsequently immersed in the $Zn(NO_3)_2/NH_4OH$ aqueous solution for 4 h at 90 °C. The fabricated MSM PDs were removed from the solution, rinsed with distilled water, and dried in air. Finally, we removed the photoresists from the interdigitated electrode surface of devices. The structure of ZnO NR MSM PD is shown in Fig. 1. On the other hand, the traditional MSM PDs with 40-nm-thick ZnO film were fabricated for comparison, where no ZnO NRs can be found.

X-ray diffraction (XRD), microphotoluminescence, and high-resolution transmission electron microscopy (HRTEM) (JEOL JEM-3010) were then used to characterize the optical and crystallographic properties of the as-grown ZnO NRs. Surface morphologies of the NRs and NR PDs were characterized by a field-emission scanning electron microscope (FESEM) (JEOL JSM-6700F). An HP-4156C semiconductor parameter analyzer was then used to measure current-voltage (*I-V*) characteristics of the fabricated ZnO NR PDs. Spectral responsivity measurements were also performed by the TRAIX 180 system with a 300 W xenon arc lamp light source and a standard synchronous detection scheme.

Figure 2(a) shows the XRD and photoluminescence (PL) results (inset) of the as-grown ZnO NR arrays. It can be seen that the ZnO NRs with good crystal quality were preferred oriented in the [002] *c*-axis direction and a strong UV emission centered at 378 nm. In Fig. 2(b), HRTEM and selective area electron diffraction (SAED) pattern show the ZnO NRs is structurally uniform and contains no defects such as dislocations and stacking with 0.52 nm *d*-spacing of (002) crystal planes.

A FESEM image with a 45° tilt angle of the ZnO NR PDs is as shown in Fig. 3; the inset shows a cross-sectional photograph of the NR arrays. The average length and diameter of these ZnO NRs were around 2.2 μm and 60–80 nm, respectively. It was found that high densities of well-aligned ZnO NR arrays were grown on the gap of interdigitated electrodes.

Figure 4 shows current-voltage (*I-V*) characteristics of the fabricated traditional ZnO film and ZnO NR MSM PDs

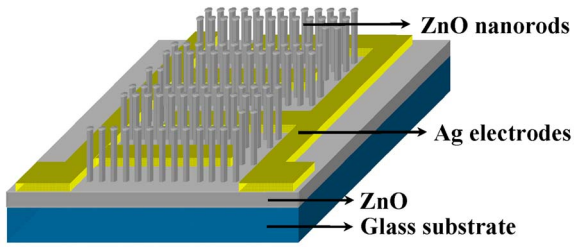

FIG. 1. (Color online) Schematic for the fabricated UV MSM PDs with ZnO NR arrays.

[a]Author to whom correspondence should be addressed. Electronic addresses: lwji@seed.net.tw and lwji@nfu.edu.tw.

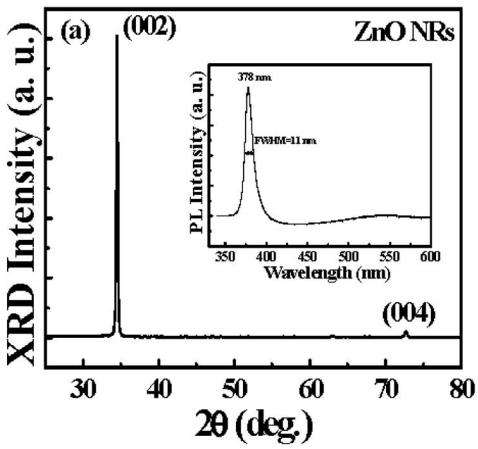

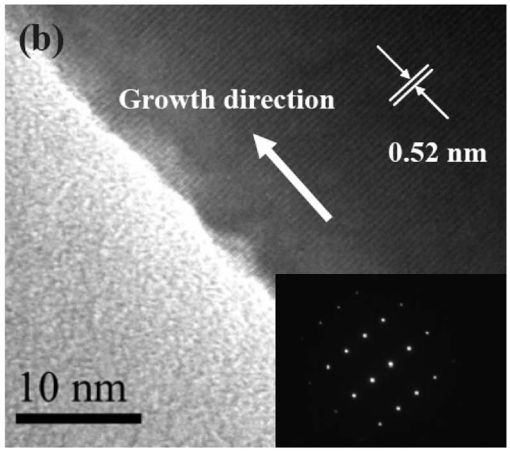

FIG. 2. (a) XRD result of ZnO NRs on ZnO/glass substrate. The inset shows the room temperature PL spectrum of ZnO NRs. (b) HRTEM image of an individual ZnO NR. The lattice spacing is 0.52 nm along the [002] direction. The inset is the corresponding SAED image.

with the Ag interdigitated electrodes measured in dark and under 370 nm illumination. With 5 V applied bias, the photocurrent to dark current contrast ratios of the ZnO and ZnO NR PDs were 1.47×10^2 and 2.99×10^3, respectively. The photocurrents generated from NR MSM PDs are increased much more than the traditional film MSM PDs could be attributed to the NR arrays having larger surface area than film.

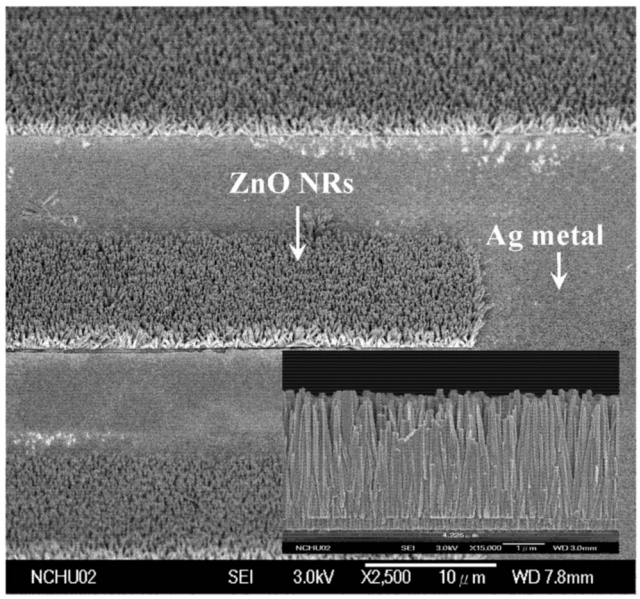

FIG. 3. FESEM image with 45° tilt angle for the ZnO NR MSM PDs. The inset shows the cross-sectional image of the ZnO NR arrays.

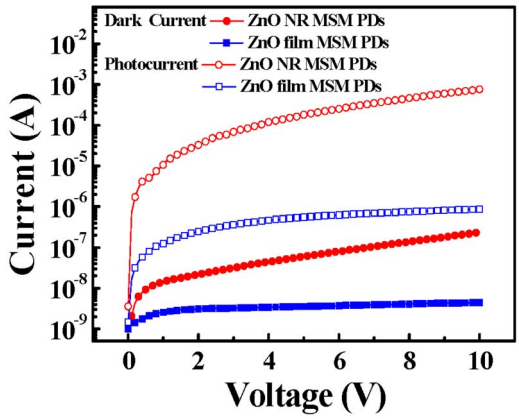

FIG. 4. (Color online) *I-V* characteristics of the NR MSM PDs measured in dark and under 370 nm illumination.

The spectral responsivities of the ZnO MSM PDs with 5 V applied bias were shown in Fig. 5. It can be seen that the photoresponsivities were nearly constant in the UV region (300–370 nm). UV-to-visible rejection ratio can be defined as the responsivity measured at 360 nm divided by the responsivity at 450 nm.[4] Table I summarizes photo-/dark current, responsivities, UV-to-visible rejection ratios for ZnO NR, and ZnO film MSM PDs. The ZnO NR MSM PDs show much higher photoresponse than the traditional ZnO MSM PDs (41.22 A/W, 0.13 A/W) can be attributed to the defects of NR surfaces, which is the origin of the trap states, and the surrounding gas molecules completely affects energy band and produce photoconduction gain.[10,11] The responsivity of a detector, R, is defined as

$$R = \frac{I_p}{P_{\text{inc}}} = \eta g \frac{\lambda(\mu\text{m})}{1.24}\text{A/W},$$

where I_p, P_{inc}, η, g, and λ are the photocurrent, the incident optical power, the quantum efficiency, the photoconductive gain, and the incident light wavelength, respectively.[17] While we apply 41.22 A/W and 370 nm to the expression, the gain can be estimated to be 1.38×10^2 by assuming $\eta=1$ for simplicity. Such a result suggests that an internal gain exists in the NR device.[10]

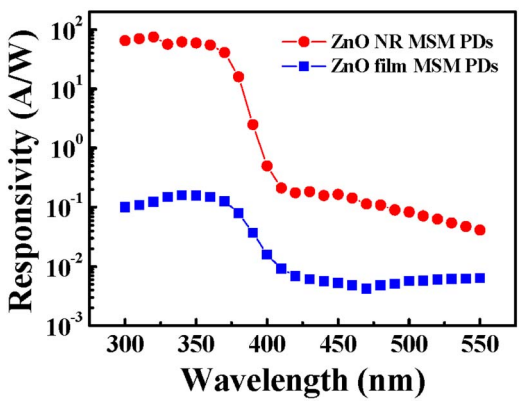

FIG. 5. (Color online) Measured spectral reponsivities of the ZnO MSM PDs at 5 V applied bias.

TABLE I. Photocurrent, dark current, photoresponsivity, and UV-to-visible rejection ratio of the ZnO MSM PDs measured at 5 V bias and 370 nm illumination.

	Photo-/dark current	Responsivity (A/W)	UV-to-visible rejection ratio
ZnO NRs	0.18 mA/60.3 nA	41.22	336.65
ZnO film	552 nA/3.55 nA	0.13	28.28

Figure 6 shows a the energy band diagram in the presence of a high density of hole-trap states at the NR surfaces. It is generally accepted that oxygen molecules are adsorbed onto the ZnO surfaces by capturing free electrons from the *n*-type ZnO $[O_2(g)+e^- \rightarrow O_2^-(ad)]$, as shown in Fig. 6(a), where a low-conductive depletion layer will be formed near the surface. The electron-hole pairs will be photogenerated $[h\nu \rightarrow e^- + h^+]$ while the photon energy of illumination is more than the energy bandgap E_g $[h\nu > E_g$, as shown in Fig. 6(b)]. The holes that migrate to the surface along the potential gradient, produced by band bending, discharge the negatively charged adsorbed oxygen ions $[h^+ + O_2^-(ad) \rightarrow O_2(g)]$; consequently, oxygen is desorbed from the surfaces, resulting in an increase in the free carrier concentration and a decrease in the width of the depletion layer.[9–11,18] In other words, the photoresponses of the NR MSM PDs are enhanced by the hole-trapping mechanism through oxygen adsorption and desorption in ZnO NRs, which increases the density of trap states. Furthermore, this leads to an increase in carrier injection and transport, producing a persistent photocurrent.

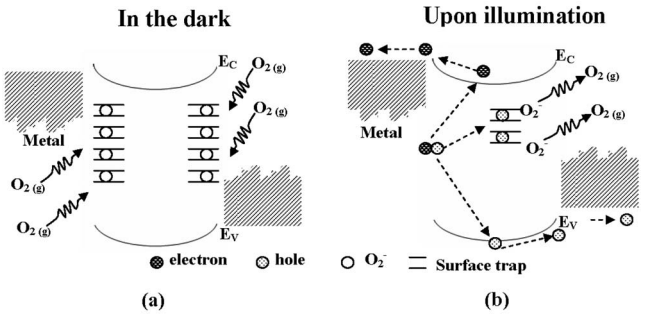

FIG. 6. Energy band illustration for photoconduction mechanism in this investigation: (a) In the dark case, oxygen molecules are adsorbed onto the ZnO surfaces by capturing free electrons $[O_2(g)+e^- \rightarrow O_2^-(ad)]$, which creates a low-conductivity depletion layer near the surface. (b) Under UV illumination at photon energy more than the bandgap $(h\nu > E_g)$, electron-hole pairs are photogenerated. The holes migrate along the potential gradient and discharge the oxygen ions $[h^+ + O_2^-(ad) \rightarrow O_2(g)]$, consequently, oxygen is photodesorbed from the surfaces.

In summary, we investigated the UV MSM PDs with selectively grown ZnO NR arrays, which show higher photoresponse compared to the traditional ZnO MSM PD. As a result, it can be attributed to the very large surface-to-volume ratios of ZnO NR arrays easily promoting oxygen adsorption and desorption at the NR surfaces. Based on the trapping mechanism related to gas adsorption/desorption, it suggests that ZnO NRs are superior materials for UV detection.

This work was supported by the National Science Council of Taiwan under Contract No. NSC-95-2221-E-150-077-MY3.

[1] D. M. Bagnall, Y. F. Chen, Z. Zhu, T. Yao, S. Koyama, M. Y. Shen, and T. Goto, Appl. Phys. Lett. **70**, 2230 (1997).
[2] D. C. Look, D. C. Reynolds, C. W. Litton, R. L. Jones, D. B. Eason, and G. Cantwell, Appl. Phys. Lett. **81**, 1830 (2002).
[3] S. J. Young, L. W. Ji, S. J. Chang, and Y. K. Su, J. Cryst. Growth **293**, 43 (2006).
[4] D. Y. Jiang, J. Y. Zhang, Y. M. Lu, K. W. Liu, D. X. Zhao, Z. Z. Zhang, D. Z. Shen, and X. W. Fan, Solid-State Electron. **52**, 679 (2008).
[5] W. I. Park, D. H. Kim, S. W. Jung, and G. C. Yi, Appl. Phys. Lett. **80**, 4232 (2002).
[6] L. W. Ji, S. J. Young, T. H. Fang, and C. H. Liu, Appl. Phys. Lett. **90**, 033109 (2007).
[7] Y. Ryu, T. S. Lee, J. A. Lubguban, H. W. White, B. J. Kim, Y. S. Park, and C. J. Youn, Appl. Phys. Lett. **88**, 241108 (2006).
[8] M. H. Huang, S. Mao, H. Feick, H. Q. Yan, Y. Y. Wu, H. Kind, E. Weber, R. Russo, and P. D. Yang, Science **292**, 1897 (2001).
[9] H. Kind, H. Q. Yan, B. Messer, M. Law, and P. D. Yang, Adv. Mater. (Weinheim, Ger.) **14**, 158 (2002).
[10] C. Soci, A. Zhang, B. Xiang, S. A. Dayeh, D. P. R. Aplin, J. Park, X. Y. Bao, Y. H. Lo, and D. Wang, Nano Lett. **7**, 1003 (2007).
[11] Y. Z. Jin, J. P. Wang, B. Q. Sun, J. C. Blakesley, and N. C. Greenham, Nano Lett. **8**, 1649 (2008).
[12] H. T. Ng, T. Yamada, P. Nguyen, Y. P. Chen, and M. Meyyappan, Nano Lett. **4**, 1247 (2004).
[13] K. Keem, D. Y. Jeong, S. Kim, M. S. Lee, I. S. Yeo, U. I. Chung, and J. T. Moon, Nano Lett. **6**, 1454 (2006).
[14] J. B. Baxter and E. S. Aydil, Appl. Phys. Lett. **86**, 053114 (2005).
[15] X. D. Wang, J. H. Song, J. Liu, and Z. L. Wang, Science **316**, 102 (2007).
[16] Q. Wan, Q. H. Li, Y. J. Chen, T. H. Wang, X. L. He, J. P. Li, and C. L. Lin, Appl. Phys. Lett. **84**, 3654 (2004).
[17] S. M. Sze, *Physics of Semiconductor Devices* (Wiley, New York, 1981).
[18] P. Sharma, K. Sreenivas, and K. V. Rao, J. Appl. Phys. **93**, 3963 (2003).